The 100-m Effelsberg Telescope and the Milky Way

Ernst Fürst

(*Max-Planck-Institute for Radioastronomy, D-53121, Bonn, Germany)*

Abstract The Effelsberg 100-m radio telescope was built almost 30 years ago for radio observations at centimeter wavelength. Observations are possible from the primary as well as the secondary focus. Some technical details of the telescope are described. Since the beginning, observations with the 100-m radio telescope contribute to all fields of radio astronomy: radio continuum, spectroscopy, pulsar research and VLBI. The telescope is well suited to map large areas of the sky in the radio continuum, in total intensity and polarization. As an example, the radio maps of the plane of the Milky Way are presented. Such data in combination with follow-up measurements at other radio frequencies provide spectral and polarization information on various objects of the Milky Way. As an example the remnants of supernova explosions are discussed. With the 100-m telescope, observations at wavelengths shorter than 1 cm become more and more important. Large feed arrays will help to speed up mapping of extended areas. A proposal exists to improve the sensitivity of the 100-m radio telescope especially at short wavelengths. Comments on this project are given.

1 The 100-m Radio Telescope

The Effelsberg 100-m radio telescope (Figure 1, Hachenberg et al. 1973) began it's astronomical operation in 1971. For about 30 years it was the largest fully steerable radio

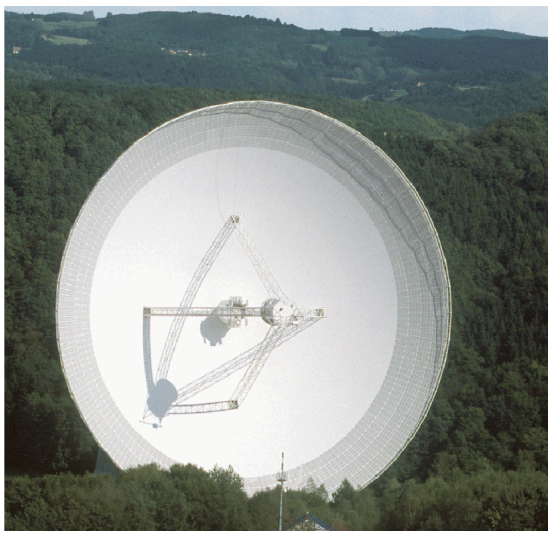

Fig. 1 The 100-m-Radio telescope Effelsberg

telescope. The telescope consists of a main paraboloid reflector of 100-m size and a gregorian subreflektor of 6.5 m size, which provides easy access to the primary (PFK) and to the

secondary (SFK) focus. In the primary focus (focal length = 30 m) only one receiver can be installed at the same time. The available receivers/frequencies range between 800 MHz and 86 GHz. A change between receivers/frequencies needs manual work. The focal length of 385m of the secondary focus allows the permanent installation of many receivers/frequencies (see Figure 2), which all are ready for observations. Optical errors are small even at large distances from the optical axis. The 100-m radio telescope is the first telescope built according to the so-called homologeous principle. When tilting the telescope from 90° to it's

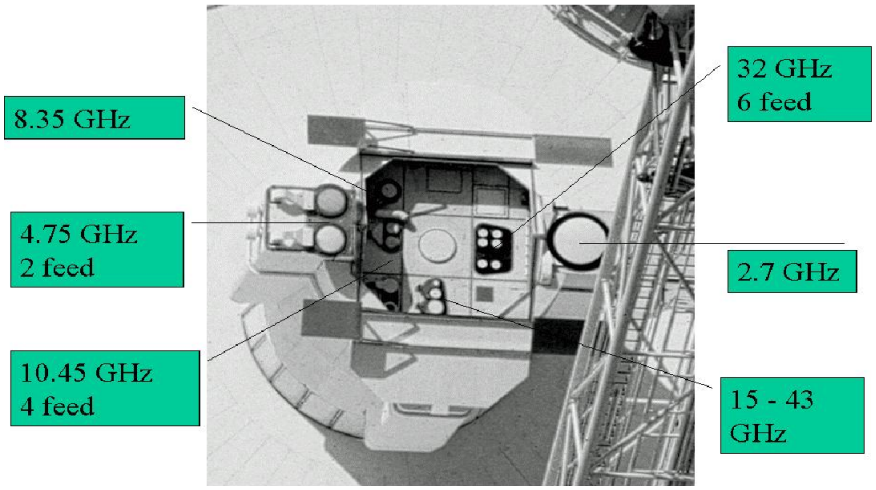

Fig. 2 The secondary focus of the 100-m-RT

lower limit of 7° elevation the maximal distortion at the edge of the reflector due to gravity is 8 cm. The best-fit paraboloid, fitted to the distorted surface, shows systematic deviations of about ±2 mm. The resulting mean deviation from the best-fit paraboloid is 0.45 mm at 32° elevation for the central region of 40 m radius. At the elevation of 32° the panels of the reflector are adjusted according to holographic measurements using geostationary satellites. Towards 90° elevation the mean deviation increases due to gravity up to 0.83 mm. The outer region of the reflector was recently filled with panels of perforated aluminium with holes of 7 mm and a filled fraction of about 50%. This part of the reflector will be adjusted during 2003. The pointing accuracy of the telescope is about 2-3 arcsec for low wind speeds. Observations have to be stopped at wind speeds larger than 16 m/s. The instrumental polarization of the telescope is usually <0.7%. For many observations a cleaning of the polarization for instrumental effects is not necessary.

Mapping of extended objects is one of the main tasks of the 100-m-RT. Over the last 30 years the 100-m-RT has contributed to the 408 MHz all-sky survey (Haslam et al. 1982) and various surveys of the Galactic plane. Nummerous individual extended Galacitc objects and external galaxies have also been mapped in total intensity and polarization. Here only the Galactic plane and supernova remnants (SNRs) are discussed.

2 The Galactic Plane and Supernova Remnants

The Galactic plane has been observed with the 100-m-RT at 2.695 MHz in the years from 1982 to 1990 (Reich et al. 1984, 1990; Fürst et al. 1990). The entire region visible from Effelsberg has been mapped. The analysis of the whole region in total intensity was finished

in 1994. The linear polarization has been analysed for the first quadrant of the Galaxy. A small section of the survey is shown in Figure 3. The various scientific goals motivating this survey were the study of HII regions and SNRs as well as the study of the extended and

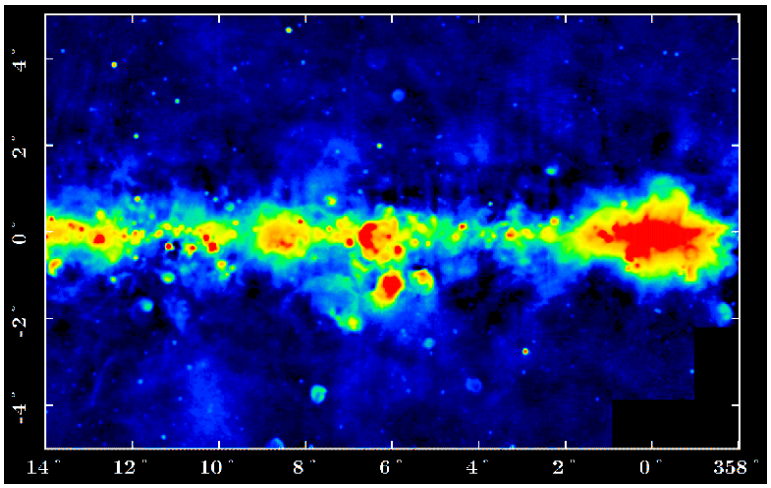

Fig. 3 Part of the Galactic plane at 2695 MHz in total intensity

diffuse emission.

2.1 Supernova remnants

An exciting example of SNRs is the well-known object S147 at the anti-centre of the Galaxy (Figure 4). The sensitive 2.695 GHz radio map corresponds even in details with

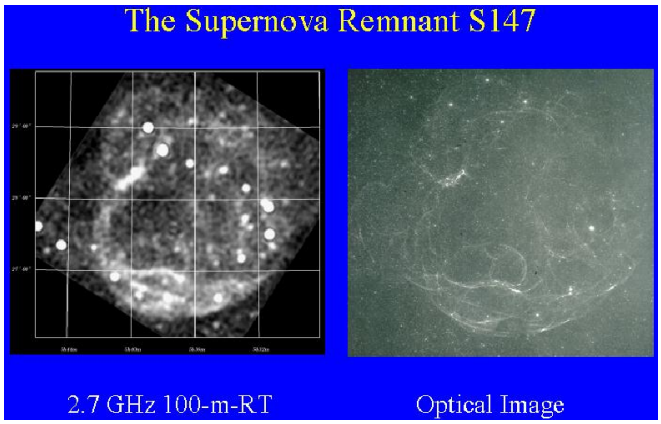

Fig. 4 The SNR S147 in radio (Fürst and Reich 1986) and optical light (van den Bergh 1973)

the optical H_α map. A pulsar is located inside the remnant, possibly associated with it (Anderson et al. 1996). It is one of few SNRs with detectable optical emission. In most cases the identification of SNRs relies on radio astronomical tools: the spectral index of the radio flux density S_ν ($S_\nu \propto \nu^\alpha$), the low infrared emission compared with HII regions, and

the radio polarization.

2.1.1 The radio flux density spectral index The radio spectrum of SNRs is typically a power

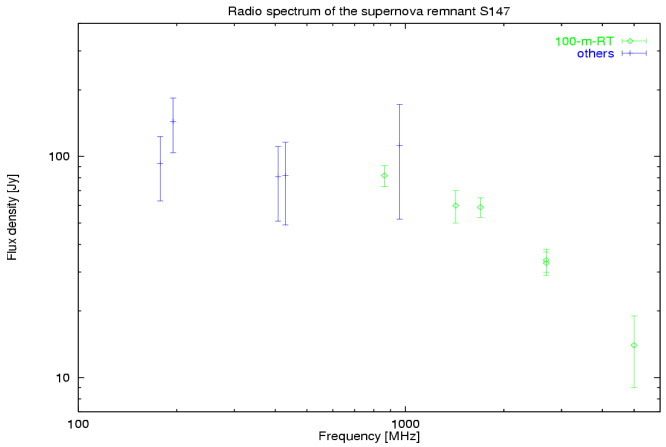

Fig. 5 The radio spectrum of S147

law with a spectral index α between -0.1 and -1.0 depending on the SNR type. In rare cases a break or bend towards high frequencies is observed. In Figure. 5 the radio flux density spectrum of S147 is shown. The power law and the spectral index are intimately related to the acceleration of electrons in the SNR shock wave, the magnetic field in the emitting regions, and the aging effects during various periods of the SNR lifetime. In case of S147 the detected emission can be separated into thin radio/optical filaments and extended diffuse emission (Fürst and Reich 1988). The spectral index maps of both components are different (see Figure 6). In Figure 6 the temperature spectral index β is used ($T_B \propto \nu^{\alpha-2} = \nu^{\beta}$).

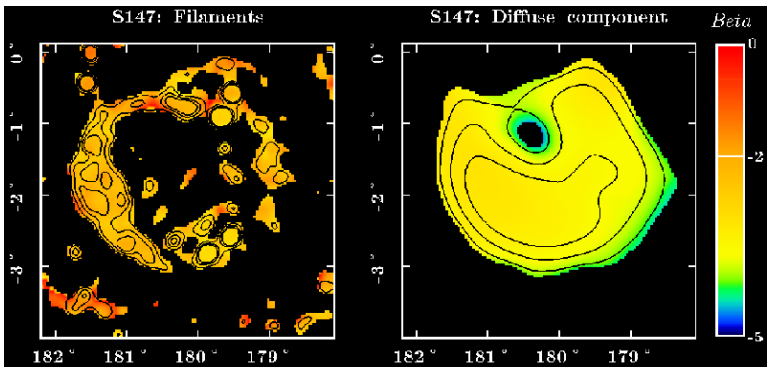

Fig. 6 The two spectral components of S147

The flux density spectral index of the filaments is close to $\alpha = -0.5$, the canonical value for Fermi accelerated electrons. The diffuse emission shows a much steeper spectrum. A possible interpretation is the exchange of electrons between filaments and the extended component and the corresponding action of compression (strong aging effects) and expansion. This mechanism may shift the possible break frequency of the extended component to low frequencies, Fürst el al. 1988).

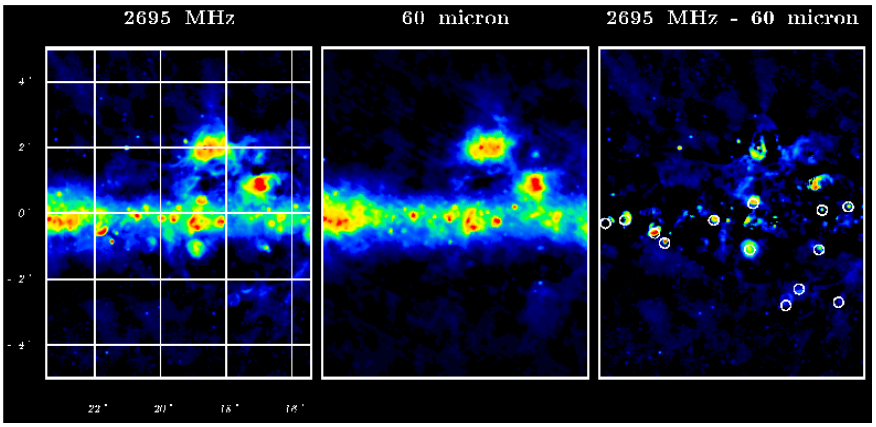

Fig. 7 The Galactic plane in radio and infrared

2.1.2 The infrared emission

The infrared emission may be used as a second tool to separate HII regions from SNRs (Fürst et al. 1987). In Figure 7 we show the radio map of a section of the Galactic plane filled with HII regions and SNRs. At 60 micron (IRAS) the region look very similar. The

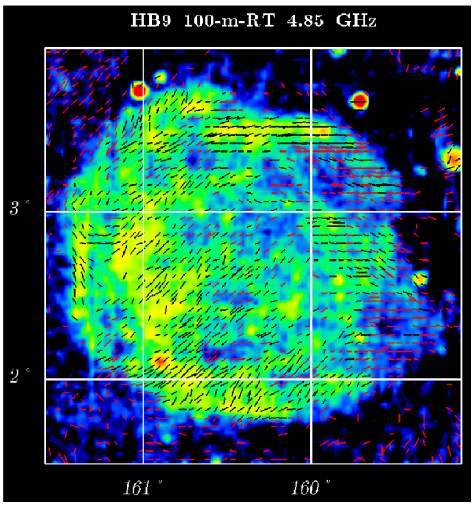

Fig. 8 The SNR HB9 in total and polarized intensity

two maps may be scaled in such a way that HII regions in the two maps have about the same amplitude. Subtracting the scaled 60 micron map from the radio map let all the HII regions disappear, while all the SNRs (circles) remain visible. Some relicts of the strong HII regions are still visible, may be as a result of intrinsic differencies between 60 micron and radio emission or small pointing differencies.

2.1.3 The linear polarization

Possibly the most convincing tool to identify SNRs is the linear polarization of the synchroton emission. One example for a polarization map of SNRs is shown in Figure 8

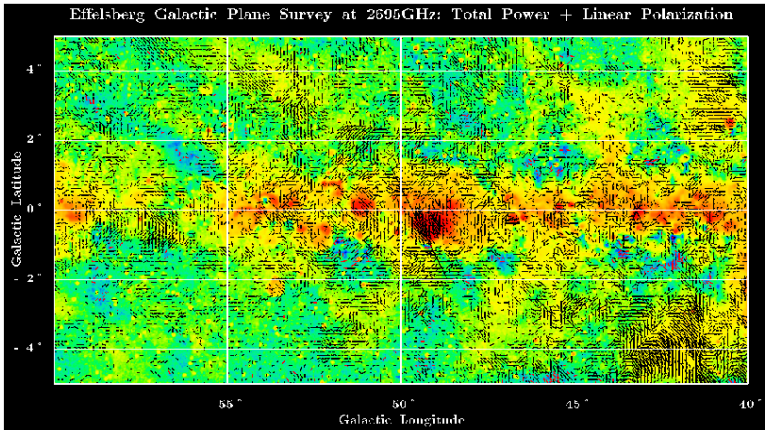

Fig. 9 Part of the Galactic plane in total and polarized intensity

(Reich et al. 1984). The linear polarization of SNRs may reach a high percentage of order 50% or more. The exact value depends on the geometry of the SNR's magnetic field as well as on the action of the Faraday effect within the source and between the object and the observer. More about Faraday effects is presented by Wielebinski and by W. Reich (this

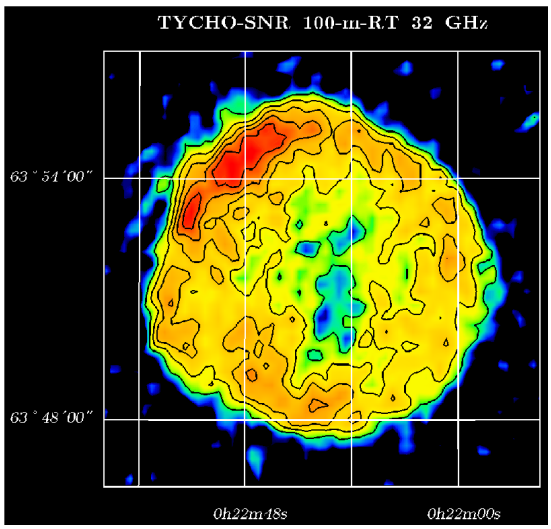

Fig. 10 Tycho-SNR at 32 GHz with the 100-m-RT

volume). In a certain sense the linear polarization of the SNR's is related to the ambient Galactic magnetic field, in particular in late phases of the SNR evolution. However, studies of the Galactic magnetic field using the Effelsberg 2695 MHz survey shows a very complicated nature of the observed field (Figure 9, Junkes et al. 1987, Duncan et al. 1999). Various effects contribute to this caotic view: Intrinsic variations of the magnetic field in intensity and direction, Faraday effects along the line of sight within the emission regions and caused by ionized gas along the line of sight or by randomly distributed Farady screens.

2.1.4 High frequency measurements

A break or bend in the SNR radio spectrum is, if any, observed at high frequencies, in most case above 10 GHz. Observations at high frequencies, particularly at 30 GHz and beyond become more and more important. New sensitive receivers at these frequencies allow mapping of extended sources in a reasonable time. As an example the SNR Tycho is shown in Figure 10 at 32 GHz. Observations at 32 GHz are made with a multi-feed system from the SFK. At present such observations are limited by a relative low antenna gain at high elevations, caused by the distortions of the not perfect homology of the main dish. The insufficient quality of the gregorian subreflektor causes an additional decrease of the gain.

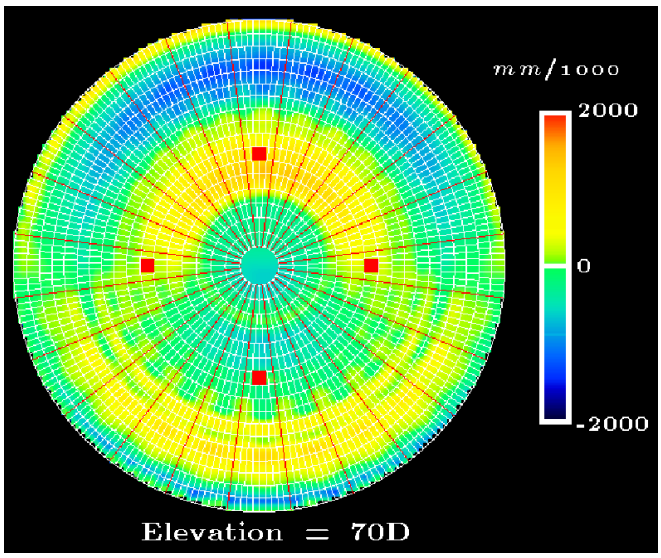

Fig. 11 The distortion of the main reflector at 70° elevation

3 Possible Improvements of the 100-m-RT

The insufficient quality of the subreflector and the remaining distortions of the homologeous main reflector contribute to a low gain particularly at high elevations. Figure 11 shows the distortions of the main reflector at the elevation of 70°. Variations of about ±2 mm are visible, which contribute significantly to the mean deviation. These deviations are uncritical for frequencies below about 10 GHz, for which the telscope was designed. Beyond 10 GHz, especially at the highest frequency of 86 GHz the beam pattern is strongly affected by these destortions. An example, the beam pattern at 86 GHz caused by these effects is shown in Figure 12. The beam pattern is calculated from the surface distortions shown in the upper left panel using common diffration theory and shows only the effect of incomplete homology. If such observation are moved to the SFK, an improvement is possible if the subreflektor is equipped with active elements. If using 96 activators the improvement of the surface and the beam pattern are shown in the right panels of Figure 12.

The following improvements are currently being discussed or in progress:

- Replacement of the subreflektor including it's mount
- Active surface of subreflector

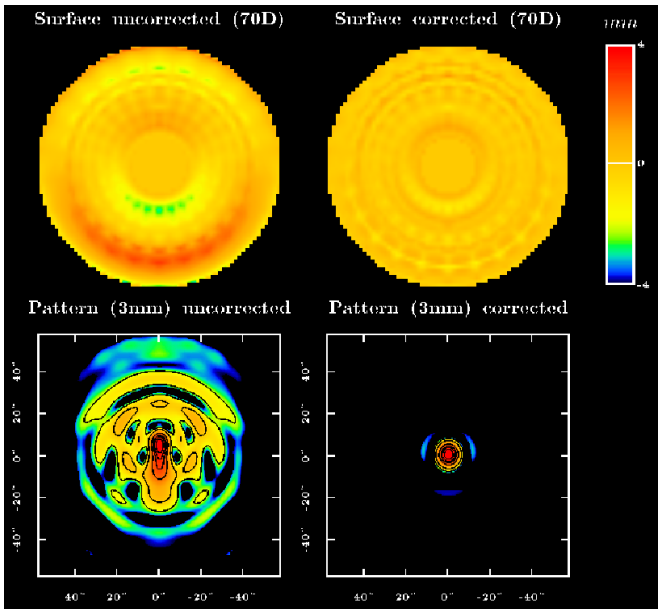

Fig. 12 The improvement of the antenna beam pattern with an active subreflector

- Automatic focus change
- Adjustment of the panels of the main reflector (Holography)
- Multichannel polarimeters
- 7-feed 21cm system for the primary focus
- 90 feed array at 32 GHz for the secondary focus

References

Anderson S.B., Cadwell B.J., Jacobe B.A., et al., ApJ, 1996, 468, L55
Duncan A.R., Reich R., Reich W., et al., A&A, 1999, 350, 447
Fürst E., Reich W., A&A, 1986, 163, 185
Fürst E., Reich W., A&AS, 1987, 71, 63
Fürst E., Reich W., in Supernova shelles and their birth events. W. Kundt ed., Lecture Notes in Physics. Springer Verlag, 1988, 316, p33
Fürst E., Reich W., A&AS, 1990, 85, 691
Hachenberg O., Wielebinski R., Grahl B.H., The 100-m radio telescope Effelsberg, Proc. I.E.E.E., 1973, 61, 1288
Haslam C.G.T., Salter C.J., Stoffel H., et al., A&AS, 1982, 47, 1
Junkes N., Fürst E., Reich W., A&AS, 1987, 350, 447
Reich W., Fürst E., Sieber W., IAU Symp, 1984, 101, 376
Reich W., Fürst E., Steffen P., et al., A&AS, 1984, 58, 197
Reich W., Fürst E., Reich P., et al., A&AS, 1990, 85, 633
van den Bergh S., Marschner A.P., Terzian Y., ApJS, 1973, 26, 19